Supporting Information（SI）

Selective capacitive removal of Pb^{2+} ions from zinc smelting wastewater using MoO_4^{2-}-intercalated CoFe-LDH electrode

Changbin Tang [a, *], Zimei Liang [a], Ting Wang [a], Yanrong Li [a], Hongjiao Xu [a], Juanqin Xue [a], Nan Zheng [b]

a School of Chemistry and Chemical Engineering, Xi'an University of Architecture and Technology, Xi'an 710055, PR China

b School of Chemistry and Environmental Science, Shaanxi University of Technology, Hanzhong 723001, PR China

*Corresponding author: Changbin Tang; mail address: tcbtop@126.com (C. Tang).

*Corresponding author

This supplementary material contains 12 pages, 2 Texts, 1 Table and 4 Figures.

Text S1 Materials and Reagents

Stainless steel mesh (1.0 mm thick, 0.1 mm aperture, denoted as SS) and graphite paper (1.0 mm thick) were purchased from Kunshan Longshengbao Electronic Materials Co., Ltd., China. Titanium dioxide (TiO_2), polyvinyl alcohol (PVA), glycerol, 1-methyl-2-pyrrolidone, polyacrylic acid, cobalt nitrate ($Co(NO_3)_2 \cdot 6H_2O$), iron nitrate ($Fe(NO_3)_3 \cdot 9H_2O$), ammonium fluoride (NH_4F), urea, and sodium molybdate ($Na_2MoO_4 \cdot 2H_2O$) were purchased from Fucheng Chemical Reagent Co., Ltd. The corresponding nitrates for preparing aqueous solutions containing lead, zinc, chromium, copper, and cobalt ions were purchased from Aladdin Reagent (Shanghai) Co., Ltd. All chemical reagents were of AR grade and were not further purified.

Text S2 Experimental Characterization

The crystal structure of each electrode coating was analyzed by X-ray diffraction (XRD, PHI-5400) operated at 40 kV with a Cu target (K_α radiation, $\lambda = 0.15418$ nm). The interlayer spacing before and after MoO_4^{2-} intercalation was calculated from the shift of the (003) diffraction peak using the Bragg equation (Formula S1). Surface morphology of the coatings was examined using field-emission scanning electron microscopy (SEM, S-4800), with elemental composition and distribution determined by an integrated energy-dispersive X-ray spectrometer (EDS). Raman spectroscopy (Horiba LabRAM HR Evolution) was

employed to obtain structural information. Chemical composition, functional groups, and valence states on the electrode surface were characterized by X-ray photoelectron spectroscopy (XPS, Thermo Scientific K-Alpha^{+}, Al K_{α} source, 1486.6 eV, 12 kW).

$$d = \frac{n\lambda}{2 \cdot \sin\theta} \qquad (S1)$$

Where, d denotes the interplanar spacing, n represents the diffraction order, λ indicates the X-ray diffraction wavelength, and θ denotes the angle between the diffracted X-rays and the crystal plane.

The electrochemical performance of the prepared electrodes was evaluated using a Corrtest 2350 electrochemical workstation. Cyclic voltammetry (CV) and electrochemical impedance spectroscopy (EIS) measurements were carried out in a 0.5 mol/L NaCl aqueous solution, with the SS/Ti_4O_7/CoFe-MoO_4^{2-}-LDH electrode as the working electrode, a platinum sheet as the counter electrode, and a saturated calomel electrode (SCE) as the reference electrode. The CV test for the SS/Ti_4O_7/CoFe-MoO_4^{2-}-LDH electrode was conducted in the potential window of -0.8 to -0.3 V (vs. SCE) at a scan rate of 100 mV/s. CV tests were also performed on Ti_4O_7/CoFe-MoO_4^{2-}-LDH and bare Ti_4O_7 electrodes in a 200 ppm Pb^{2+} solution at the same scan rate. Furthermore, the Ti_4O_7/CoFe-MoO_4^{2-}-LDH-180 electrode was tested at various scan rates ranging from 10 to 100 mV/s. EIS measurements were performed at the open-circuit potential over a frequency range of 0.1 Hz to 100 kHz, applying a sinusoidal potential perturbation with an amplitude of 5 mV. Galvanostatic charge-discharge (GCD) tests were run at a current density of 0.5 A g^{-1}, and the specific

capacitance (C, F g^{-1}) of the electrode was calculated from the constant-current discharge segment using Equation (S2).

$$C_p = \frac{I \cdot t}{m \cdot \Delta V} \qquad (S2)$$

Where C_P denotes specific capacitance (F g^{-1}), I represents current (A), m indicates active material mass (g), t denotes discharge time (s), and ΔV is the potential window (V).

The electroadsorption experiment utilized a CDI apparatus[1] designed, assembled, and fabricated by the research group. This apparatus comprised an adsorption module (including an anode, cathode, silica gel spacer, PMMA separator, and acrylic plate), a peristaltic pump, a storage tank, a conductivity meter, and a DC power supply. The experiment was conducted under continuous feed mode. During the experiment, distilled water was continuously pumped into the CDI adsorption module at a flow rate of 10 mL min^{-1} using a peristaltic pump until the effluent conductivity stabilized. Subsequently, the electroadsorption experiment was conducted using an electrode with an active material loading of 25 mg, and 100 mL of 50 ppm Pb^{2+} solution was introduced into the reservoir. A designated voltage was applied across the electrodes using a DC regulated power supply, and the entire electroadsorption process was maintained at room temperature (25 °C). The electrode plate spacing was set at 2 mm. The effects of varying applied voltages and pH values on Pb^{2+} removal performance were investigated within the ranges of DC voltage (0.8-1.6 V) and solution pH (2–10). Solution pH was adjusted using 1 mol/L NaOH and 1 mol/L HNO_3, respectively.

For testing the selective removal of Pb^{2+} by the electrode, a multi-ion mixed solution containing Pb^{2+}, Cu^{2+}, Zn^{2+}, Cd^{2+}, and Co^{2+} was selected, with each ion present at concentrations of 10 ppm and 50 ppm. All electroadsorption processes reached equilibrium at 150 min (at which point conductivity remained essentially stable). The concentrations of each experimental ion after adsorption were precisely measured using an inductively coupled plasma mass spectrometer (Agilent 8900). Adsorption characteristics were evaluated based on adsorption capacity, removal efficiency, and the relative removal coefficient for Pb^{2+}. Additionally, real wastewater generated during the acid production and waste acid purification processes from the Shangluo Zinc Smelter (Shangluo, China) was collected. First, to prevent organic pollutants in the wastewater from contaminating the electrodes, anodic oxidation[2] was employed to reduce the COD from 85.67 mg/L to 6.37 mg/L. Based on this, electroadsorption experiments were conducted using optimized process parameters. Prior to electroadsorption, the actual wastewater was analyzed, showing concentrations of Pb^{2+} at 0.328 ppm, Zn^{2+} 13.277 ppm, Cd^{2+} 0.187 ppm. Adsorption performance was evaluated based on parameters including adsorption capacity, adsorption time, Pb^{2+} removal rate, and relative removal coefficient.

The adsorption capacity of ions is calculated according to formula (S3):

$$AC = \left(C_0 - C_t\right) \times \frac{V}{m} \#(S3)$$

Where, C_0 denotes the initial concentration of the ion (mg L^{-1}), C_t denotes the equilibrium concentration of the ion (mg L^{-1}), V denotes the total volume of the solution (mL), and m denotes the mass of the electrode active substance (g).

The ion removal efficiency is calculated using formula (S4):

$$Re = \frac{C_0 - C_t}{C_0} \times 100\% \#(S4)$$

Where, C_0 denotes the initial concentration of the ion (mg L^{-1}), and C_t denotes the equilibrium concentration of the ion (mg L^{-1}).

The relative removal coefficient of Pb^{2+} is calculated using formula (S5):

$$S = \frac{RE_{Pb}}{RE_B} \#(S5)$$

Among these, RE_{Pb} and RE_B represent the removal efficiencies of Pb^{2+} and other ions (Cu^{2+}, Co^{2+}, Cd^{2+} and Zn^{2+}), respectively.

Table S1 Comparison of Relative Removal Coefficients for Pb^{2+} and Other Ions During Electroadsorption of Mixed Heavy Metal Ions (10 ppm and 50 ppm) Using Ti_4O_7/CoFe-MoO_4^{2-}-LDH

ion	10 ppm	50 ppm
Pb/Cu	10.92	3.01
Pb/Zn	14.62	6.16
Pb/Cd	21.64	3.69
Pb/Co	45.43	17.98

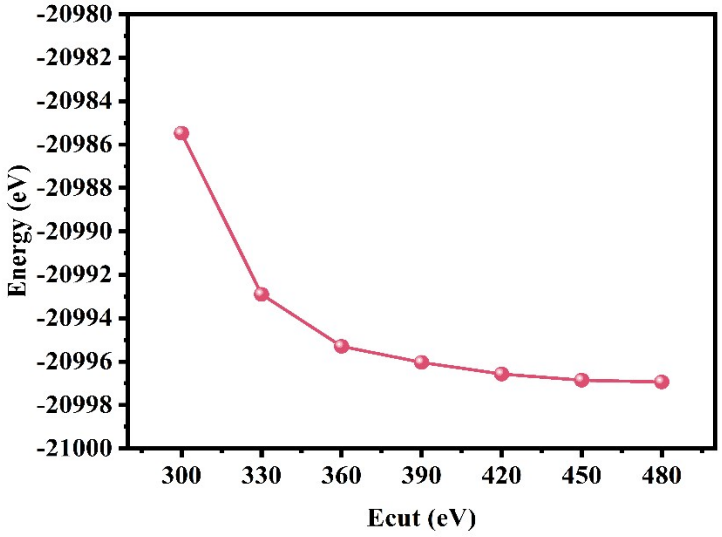

Figure S1 Convergence of the total energy as a function of the plane-wave cutoff energy (E_{cut}).

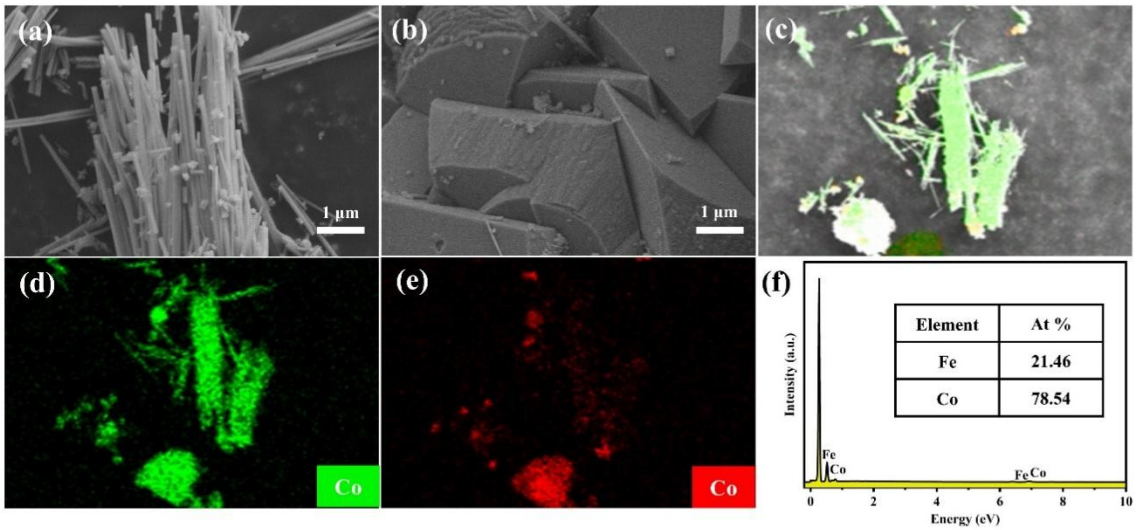

Figure S2 Surface morphology and high-magnification photographs of CoFe-LDH (a) and Ti_4O_7/CoFe-MoO_4^{2-}-LDH-120 (b); (c–f) EDS elemental maps and elemental contents of CoFe-LDH.

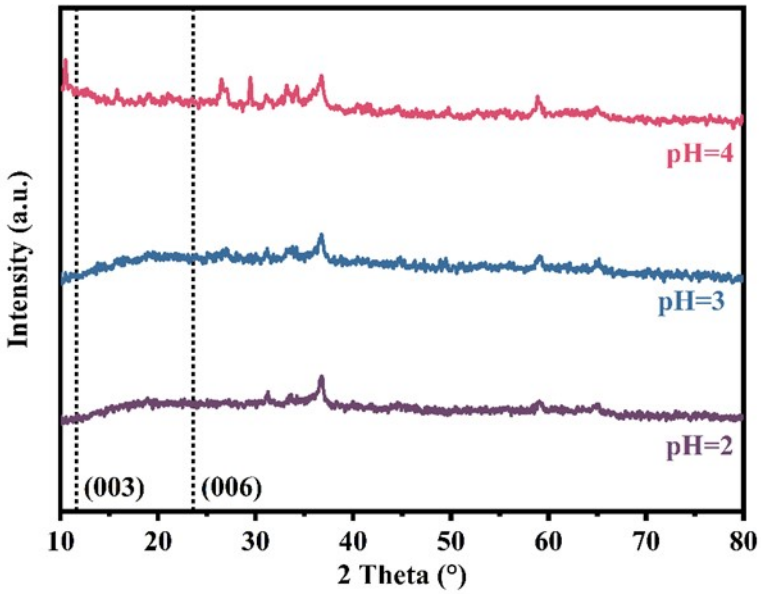

Figure S3 XRD patterns of CoFe- MoO_4^{2-}-LDH treated at different pH values.

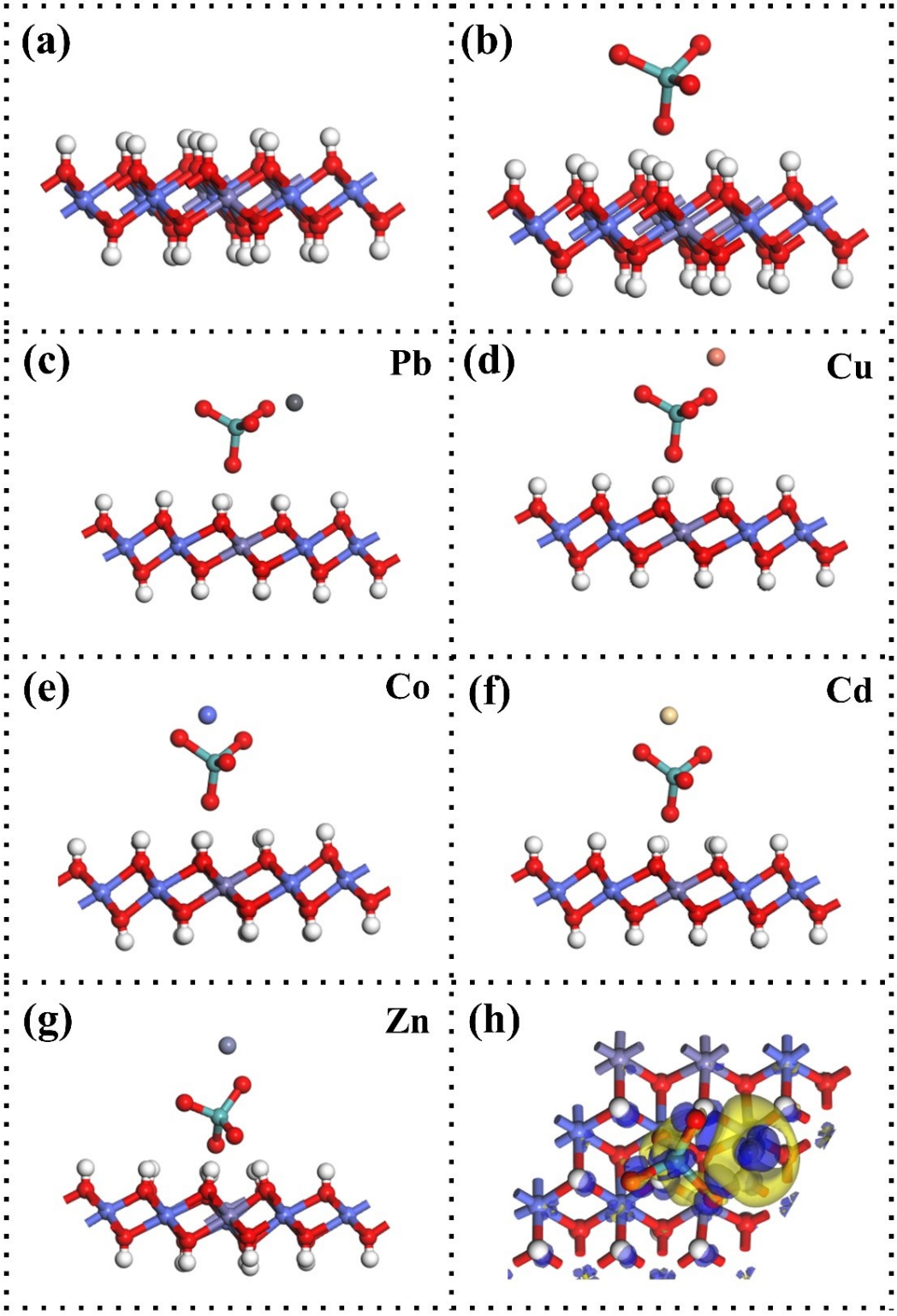

Figure S4 Original models of CoFe-LDH (a) and CoFe-MoO_4^{2-}-LDH (b), adsorption models for (c) Pb, (d) Cu, (e) Co, (f) Cd, and (g) Zn; (h) 3D top view of the differential charge density for Pb adsorbed between the layers of CoFe-MoO_4^{2-}-LDH. Blue regions indicate gained electrons, while yellow regions indicate lost electrons.

References

1 C. Tang, Y. Yu, Y. Shi, Y. Li, Y. Zhang and J. Xue, *Phys. Chem. Chem. Phys.*, 2023, **25**, 18454–18464.

2 C. Tang, X. Guo, W. Zhang, Y. Yang, L. Yu, J. Xue, X. Yin and N. Zheng, *Sep. Purif. Technol.*, 2025, **363**, 132077.